ACS Biomaterials SCIENCE & ENGINEERING

pubs.acs.org/journal/abseba

Article

Development of a Microfluidic Droplet-Based Microbioreactor for Microbial Cultivation

Chee Meng Benjamin Ho,[▽] Qi Sun,[▽] Adrian J. T. Teo, David Wibowo, Yongsheng Gao, Jun Zhou, Yanyi Huang, Say Hwa Tan,* and Chun-Xia Zhao*

Cite This: *ACS Biomater. Sci. Eng.* 2020, 6, 3630−3637

Read Online

ACCESS | Metrics & More | Article Recommendations | Supporting Information

ABSTRACT: Droplet microfluidics creates new opportunities for microbial engineering. Most microbial cultivations are carried out in bioreactors, which are usually bulky and consume a large amount of reagents and media. In this paper, we propose a microfluidic droplet-based microbioreactor for microbial cultivation. A microfluidic device was designed and fabricated to produce many droplet-based microbioreactors integrated with an AC electric field for the manipulation of these microbioreactors. Droplets encapsulating fluorescent *Escherichia coli* cells were generated, sorted, and trapped individually in small chambers. Fluorescence intensity was monitored to determine cell growth. An electric field with varying voltages and frequencies manipulates the droplets, simulating an oscillation effect. Initial results showed that electric field does not affect cell growth. A comparison with shake flask showed that a similar standard growth curve is obtained when cultivating at room temperature. This device has the potential for making droplet-based microbioreactors an alternative for microbial engineering research.

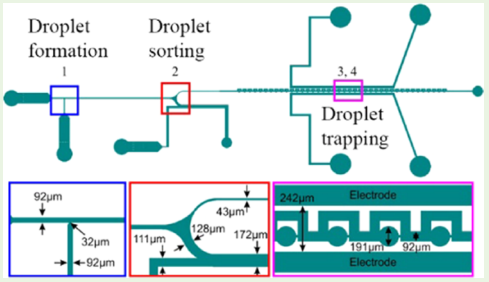

KEYWORDS: *microbioreactor, microfluidics, E. coli, oscillation and AC electric field*

INTRODUCTION

Bioreactors are important tools for cell culture and fermentation in which researchers can gain better insights into the functions of microorganisms at molecular and genetic levels.[1] The ability to effectively control various bioprocess conditions in bioreactors, such as temperature, pH, agitation, and dissolved oxygen (DO) levels,[2−4] results in valuable physiological and metabolic information at different stages of the fermentation process.[1] Although conventional automated stirred-tank bioreactors provide extensive control over the cell culture environment, reliability, and generation of information-rich data, they are typically too expensive and labor-intensive for screening purposes. Bench-scale bioreactors, despite their improvement in recent years with the reduction of reactor volume and the increase in the number of parallel operating reactors,[5] remain expensive due to the sophisticated measurement devices inherent in them and the time-consuming efforts for sterilization and sensor calibration. Simple bioreactors, i.e., test tubes, shake flasks, and microplates, are nonetheless still widely used in laboratories.[6−8] The main advantages of microplates (typically containing 24 or 96 parallel wells) are their small working volumes (typically ranging from 0.1 to 3 mL per well[9,10]), high throughput, and automated experimental setup. However, the microplates have limited control over the bioprocess conditions, and the data obtained are often limited to endpoint measurements. Therefore, there is currently a gap for further development of microplates as high-throughput microreactor systems with extended measurement points and parameter controls.[1]

Microbioreactors with integrated sensors combining the small volumes of microplates with the monitoring and control features found in bench-scale systems represent a promising tool for rapid, high-throughput, and cost-effective screening.[1] If a bioreactor could be miniaturized into the micrometer scale, it would bring about numerous new applications, such as biosensors, microfermentor arrays, or microbiological assay kits. A possible technology to make that happen would be using microfluidics. While most microfluidic research efforts to date have concentrated on eukaryotic cell biology,[11,12] microfluidics is slowly making its impact on microbiology.[13,14] Its scale of size matches well with the physical dimensions of most microorganisms, and micron-scale tools enable various manipulation on individual cells and their immediate extracellular environments (referred to as the microenvironment), shape, and internal organizations.[13,15] Most microfluidic devices are fabricated using soft lithography with poly(dimethylsiloxane) (PDMS). Soft lithography provides a fast and versatile fabrication technique, while PDMS provides

Received: February 27, 2020
Accepted: May 5, 2020
Published: May 5, 2020

attractive materials properties such as biocompatibility, transparency, and flexibility.[16,17] Microfluidics is expected to play several significant roles in advancing microbiology by precisely controlling the local microenvironments surrounding microbial cells, by isolating and studying individual or small groups of cells, and by providing identical and reproducible culture conditions and therefore generating quantitative data.[1,6] This is further shown with microbial microbioreactors where applications focus on screening strains and examining growth parameters.[18−26]

An integrated microfluidic microbioreactor (μbr) indeed has clear advantages such as small volume, single use, and high throughput. However, it is important to bear in mind that most reactors involve one reaction and require extensive handling of tubing when the scale increases. Recently, droplet microfluidics has become one of the key technologies that is opening up new experimental possibilities in biology.[6] It offers numerous advantages by encapsulating cells in individual droplets.[27] First, a single cell can be isolated into its own tiny liquid compartment. These stochastic confinements allow biochemical products secreted by cells to accumulate faster compared to cells that live in a bulk culture, thereby reducing biochemical production times. Second, the ability to upscale from a few to thousands of droplets allows droplet microfluidics to be a high-throughput analyzing tool that is versatile and powerful.[28−30] Finally, it offers precision control of the local environment, enabling researchers to study topics related to growth, mobility, adhesion, and chemical communication of cells, as well as the collective behavior and response of a cell population, which in turn offers brand-new scientific knowledge.[31,32]

In this paper, we developed a droplet-based microfluidic microbioreactor for microbial cultivation. For this μbr, we used a T-junction for generating uniform monodisperse droplets that encapsulated a small number of bacteria. The design contained individual traps that allowed capturing of sorted droplets while preventing their coalescence with the following droplet. Once a suitable device had been fabricated, microorganism compatibility and device performance were evaluated using engineered *Escherichia coli* producing green fluorescent protein (GFP). Droplet size and bacteria viability images and videos were all captured using a fluorescence camera and analyzed using a customized written program by MATLAB. For manipulating the droplets, an electric field with square-wave modulation was applied, giving an oscillation effect on *E. coli*. Our initial results showed that *E. coli* could grow normally in both static and oscillating droplets. A stable growth of *E. coli* was also achieved with the use of our droplet-based microfluidic μbr device compared to the use of a shake flask. This shows that our microfluidic device is stable and possesses the possibility of upscaling for further applications. The development and utilization of this device for culturing and investigating the growth of microorganisms represent the first step in realizing a fully integrated device toward high-throughput microorganism fermentation.

MATERIALS AND METHODS

Fabrication of the Microbioreactor Device. The microfluidic devices were fabricated using standard photolithography and soft lithography techniques[33,34] with SU-8 (Microchem SU-8 3050) and PDMS (Sylgard 184, Dow Corning), respectively. Briefly, SU-8 was spin-coated (Laurell WS-650-23 B) at 1100 rpm for 30 s and dried at 95 °C for 40 min. This baked wafer was then exposed to UV light for 5 s with a patterned mask and baked at 95 °C for 7 min. Unpolymerized regions of the SU-8 were removed by soaking and spraying the wafer with the SU-8 developer. This protocol gives us a depth of approximately 100 μm. Replicas of this mold were patterned using PDMS in the standard 10:1 ratio (silicone elastomer base/curing agent) and heated to 80 °C for at least 1 h. The inlets and outlets of the PDMS device were punched and washed with isopropanol before being irreversibly bonded to a glass chip with an oxygen plasma activation. Electrodes were made using an indium alloy (Indium Corporation) for the generation of an AC electric field. Chips were surface-treated with Aquapel (PPG Industries) through the inlets, and the residues after the surface treatment were flushed out with pressurized air.

Bacterial Strain, Growth Media, and Cultivation Conditions. *E. coli* producing green fluorescent protein (GFP) (ATCC 25922GFP) was purchased from the American Type Culture Collection (ATCC, Manassas, VA). This strain was selected in this study due to the relative ease of recombinantly producing the GFP and the ability to easily quantify fluorescence intensities in cell cultures. To cultivate *E. coli*, a single colony selected from a freshly streaked Luria-Bertani (LB) agar plate (10 g/L tryptone (BD Biosciences, Australia), 5 g/L yeast extract (Merck, Australia), 10 g/L NaCl (Chem-Supply, Australia), and 5 g/L agar (Amresco)) was inoculated into 5 mL of LB media (10 g/L tryptone, 5 g/L yeast extract, and 10 g/L NaCl) and incubated at 30 °C with shaking at 150 rpm overnight. The overnight cell culture (1 mL) was seeded into a 50 mL falcon tube containing 10 mL of fresh LB media and then incubated at 37 °C and 150 rpm until the optical density at 600 nm (OD_{600}) reached approximately 0.6 before loading the cell culture into the microfluidic device. All media for bacterial cultures were sterilized by autoclaving at 121 °C for 15 min, and after cooling, they were supplemented with 100 μg/mL ampicillin (Gibco).

Microfluidic Setup. Before the start of each experiment, a new fully functional microfluidic device was mounted onto an inverted microscope (Nikon Ti-E, Japan) equipped with two cameras to capture the video (Phantom Miro 3, Vision Research, Inc.) and the fluorescence images (TrueChrome Metrics, Tucsen). A heating glass (HG-S-Z001, Live Cell Instrument) was adapted on the microscope stage for controlling and maintaining a constant temperature throughout the experiments. Two temperature settings, 27 and 40 °C, were used in this setup, which maintained the device temperature at 25 and 37 °C, respectively. PTFE tubings were connected to the inlets of the device, with the other end connected to the glass syringe. Three glass syringes were used: one channel is for the dispersed phase *E. coli* GFP suspensions and the other two channels are for the continuous-phase mineral oils (cat. no. M5904, Sigma-Aldrich, Australia) with 2 wt % of Span 80 (cat. no. S6760, Sigma-Aldrich, Australia). The glass syringes were all controlled with syringe pumps with adjustable flow rates (NEMESYS). For generating an electric field, the device was connected to an alternating-current electric generator (33210A, Agilent) and an amplifier for electrical modulation. Each experiment was repeated three times, with images and a 1 min recording of five control droplets and five experimental droplets taken at 30 min intervals. The 1 min video will then undergo video processing by taking the brightness from each frame and getting an overall average. Two types of images, i.e., fluorescent and white lights, were captured. For the images and video, each droplet boundary has to be clearly seen and that plane is fixed and returned at each interval. The images were then processed using a customized MATLAB program to determine the fluorescence intensities.

Image Analyses. Images and videos obtained from all experiments were recorded and analyzed using MATLAB. To measure the fluorescence intensity, a binary mask was needed for extracting the location and size of the droplet, which can be operated both automatically or manually. For the automated process, droplet images from the white light images were detected as circles using the Circular Hough Transform (CHT) algorithm, which is robust to noise, occlusion, and varying illumination. Once the droplet was detected, the CHT algorithm may return multiple results (circles) for each droplet. An interactive process was developed so that the user can

https://dx.doi.org/10.1021/acsbiomaterials.0c00292
ACS Biomater. Sci. Eng. 2020, 6, 3630−3637

select the best circle from top 10 candidates provided. The circle chosen was then given as a binary mask. If the circle could not be detected, the image segmentation technique would be used to trace the outline of the droplet before converting it to a binary mask. The fluorescence videos or images corresponding to their own binary mask were then analyzed. The data files were first converted from color images into grayscale images. The mean values of the grayscale images were calculated based on the area covered by the binary mask generated earlier. The output indicated the fluorescence intensity. For the video files, the program processed each frame and calculated its intensity. It is important to note that the binary mask must be applied to each droplet individually, while the calculation steps can run automatically. The code will be shared upon request.

RESULTS AND DISCUSSION

Design of the Droplet-Based Microfluidic μbr Device.

In this study, a droplet-based microfluidic μbr device was designed to form water droplets encapsulating bacteria cells and developed as a bioreactor for the microbial cultivation. Recombinant *E. coli* producing green fluorescent protein (*E. coli* GFP) was used as a model bacterium. To cultivate *E. coli* GFP, the μbr device was designed to consist of four key components: (1) droplet generation, (2) droplet sorting, (3) droplet trapping, and (4) droplet oscillation (Figure 1). In the droplet generation component, a T-junction was used to mix a continuous oil phase (mineral oils containing 2% of Span 80) and a dispersed water phase (*E. coli* GFP in an LB medium), thus forming water-in-oil emulsion droplets encapsulating *E. coli* GFP (Figure 1, blue box). To sort droplets of uniform size, an additional fluidic inlet (secondary mineral oil) was introduced at a controlled flow rate to assist in sorting the droplets and direct them to the upper channel (Figure 1, red box). The sorted droplets were flowed further entering the droplet trapping region, which contained a total of 40 traps near the electrodes, of which 10 were located before the electrodes, 20 were in between the electrodes, and 10 were located after the electrodes. The enlarged image (Figure 1, purple box) shows the design of droplet trapping compartments. Additionally, in this droplet trapping region, an exhaust channel built at the back of the trap allowed the continuous oil phase to flow through when the trap was empty. Once a droplet was trapped, the exhaust channel caused the emulsion flow to terminate and another droplet to enter.[35] The droplets trapped in between the electrodes were exposed to an AC electric field of various frequencies and amplitudes deforming the droplets at a constant speed and creating oscillation effects (Figure 1, purple box).

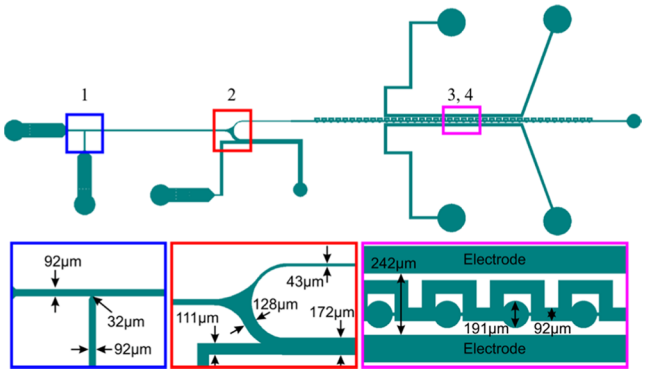

Figure 1. Microchip design and its critical dimensions. (1) Blue boxes: The T-junction for water-in-oil droplet formation with the dimensions shown for the continuous-fluid channel and the dispersed-fluid orifice. (2) Red boxes: The structure of droplet sorting with the curved-path dimensions. (3, 4) Purple boxes: The structures of both droplet trapping and droplet oscillation regions along with the dimensions of continuous-fluid channel, traps, and a gap between both electrodes.

To generate water-in-oil droplets in the microfluidic T-junction, the flow rates of the continuous phase (Figure 2a, orange) and the dispersed phase (Figure 2a, blue) were controlled at 150 and 30 μL/min, respectively. At this stage, the droplet size can be varied by controlling the initial flow rates of water and/or oil phase (Figure 2b). Before entering the droplet sorting region, the droplets from the droplet generation region would be decelerated due to the increase in the channel size and exited through the lower channel following the default streamline in which it was positioned. A secondary oil phase was then introduced for sorting the droplets achieving a uniform size of droplets as well as for directing the droplets into the designated chambers using hydrodynamic actuations. By controlling flow rates of the secondary oil between 1000 and 6500 μL/min, the flow rate of droplets could be slowed down and the flow streamline could be changed to the opposite direction, thus causing droplets from different directions to collide with each other and to force some droplets moving into the upper channel (Figure 2c). Further increasing the flow rate of the secondary oil to higher than 6500 μL/min caused all of the droplets to flow into the upper channel, eventually followed by droplet coalescence, hence diminishing the droplet sorting capability (Figure S1). In the upper channel, the droplets were trapped individually into individual chambers before the flow rates of the fluids were reduced to 10 μL/min (Figure 2d). In this way, the trapped droplets could be prevented from flowing back into the sorting chamber. The trapped individual droplets encapsulated with bacteria were then exposed to an AC electric field using a 50 kHz sine wave with varying electrical

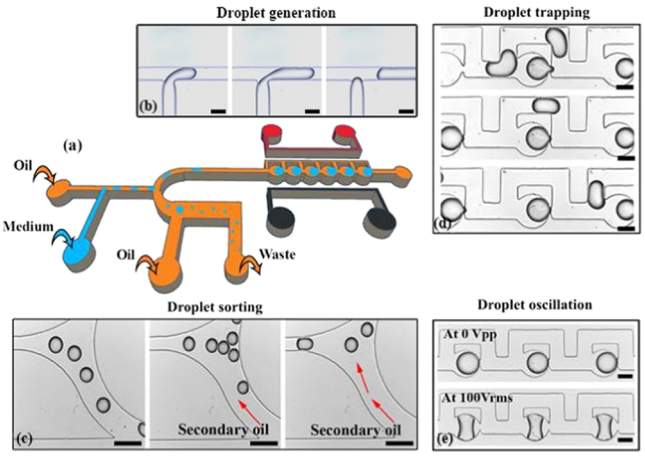

Figure 2. Microfluidic microbioreactor (μbr) for droplet formation, sorting, trapping, and oscillation. (a) Schematic illustration of the droplet-based microfluidic platform. The platform consists of four main components: (b) droplet generation; (c) droplet sorting: flowing the secondary oil at a controlled flow rate sorted the droplets to a uniform size and simultaneously changed the droplet flow direction toward the upper channel as indicated by the red arrows; (d) droplet trapping; and (e) droplet oscillation under the AC electric field at 100 V_{rms}, which caused the trapped droplets to deform. Scale bar = 100 μm.

https://dx.doi.org/10.1021/acsbiomaterials.0c00292
ACS Biomater. Sci. Eng. 2020, 6, 3630−3637

amplitude (100−400 V_{rms}) and square modulation frequency (1−100 Hz), providing a dynamic environment for cells to grow (Figure 2e).

Characterization of μBr. As droplets act as a microreactor for *E. coli* cultivation, it is important to maintain the reaction volume or to characterize any volume variation. An initial droplet stability test was performed using droplets of approximately 120 μm diameter, which were deposited in the integrated trap structures and incubated at 37 °C for 100 min (Figure 3a−h). The images of droplets were taken at 10 min intervals, and the droplet volume percentages were measured and calculated using our customized MATLAB program and ImageJ for verification (procedures can be found in S2). The results clearly showed that the droplet size slowly decreased over 100 min, with a 50% decrease at 90 min (Figure 3a−i). Droplet size plays an important role in the fluorescence experiment as we want to ensure that the fluorescence intensity is due to the increase in cell growth rather than the accumulation of GFP when the droplet shrinks. Droplet shrinkage is mainly due to the porosity of the PDMS matrix, the shearing by continuous-phase flow rate,[35−37] and the evaporation (as the device temperature was maintained at 37 °C to provide an optimal growth condition for *E. coli*). To assess cell viability and protein expression within the droplet, *E. coli* containing a multicopy vector encoding the green fluorescent protein (GFP) mut3 was used. Due to the mutation in the GFP, its fluorescence intensity can be detected within 8 min after induction of the *E. coli* growing in the log phase, compared to wild-type GFP, which is detectable after 1−2 h of growing *E. coli* under identical conditions.[38] This coupled with the doubling time of the *E. coli* of approximately 15−20 min allowed us to monitor the fluorescence intensity at least for two cell cycles. Droplets were imaged at every 10 min interval, and the fluorescence intensity was measured. Figure 3j−r shows the increase of fluorescence intensity after 20 min, indicating that the bacteria were able to proliferate, and the shrinkage of droplets did not affect their growth after 40 min. It was previously shown that fluorescent protein did not leak out of the continuous phase thus allowing us to continue monitoring the bacteria within the droplet.[35] Based on this result, for the observation of *E. coli* growth, the flow rate of the continuous phase was increased from 30 to 40 μL/min, which also caused the droplet size to increase from 150 μm to approximately 180 μm, respectively. This would generate a droplet volume of 2.2 nL, which has about 600 cells encapsulated in the droplet. While lowering the temperature to 25 °C caused the rate of droplet shrinkage to decrease, this gave us enough time (∼3 h) to properly observe at least a few growth cycles of *E. coli* to obtain a substantial result.

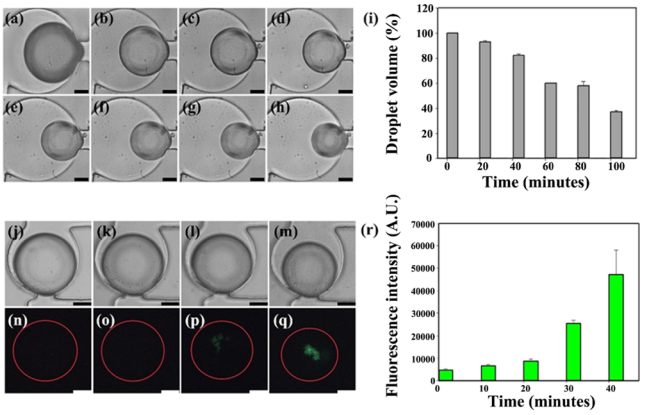

Figure 3. Droplet stability over time at 37 °C and bacteria viability testing. (a−i) A decrease in droplet volume was observed over a period of 100 min. (a−h) Images of droplet size; (i) volume percentage decrease over a period of 100 min; (j−r) fluorescence intensity over time for 40 min; (j)−(m) white light images of droplets; and (n−q) fluorescence images of encapsulated bacteria. The scale bar represents 50 μm.

To observe and analyze *E. coli* growth in the immobilized droplets, the intensity of GFP generated was quantified using epifluorescence microscopy. Droplets were constantly observed with a fluorescence camera. The evaluation processes of images and videos were automated to aid us in speeding up the processes. As a result, settings for the images were maintained constant and characterized before any experiment. Important factors such as camera settings as well as microscope settings were taken into consideration. The camera settings were determined using the default setting of the camera initially (as the control). Normal and fluorescence images of encapsulated bacteria droplet were taken before changing the camera settings one at a time while capturing new images. Different camera settings were then compared against the control. The camera was manually set, and the automatic function was not used to determine the optimal setting. Our results showed that exposure (the amount of time the cells are exposed to light), gain (light sensitivity of the camera), contrast (difference in color and brightness), and γ (value of pixel relates to actual brightness) played a significant role in affecting our images for

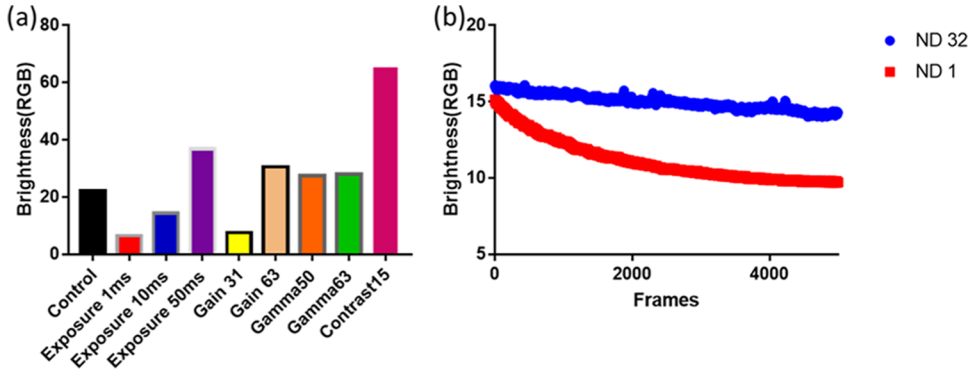

Figure 4. Characterization of the camera and fluorescence settings that may affect the overall results for the system. (a) Camera settings (exposure, gain, γ, and contrast) and (b) fluorescence lamp transmittance power (ND32 and ND1) for 1.5 h of exposure.

https://dx.doi.org/10.1021/acsbiomaterials.0c00292
ACS Biomater. Sci. Eng. 2020, 6, 3630−3637

different experiments (Figure 4a), whereas other camera settings, including saturation and sharpness, did not (Figure S2). Furthermore, as the fluorescent bacteria were freely moving in the droplet, images of the droplet at different *z*-planes (set as the microscope setting) were captured for observing whether this movement might affect the readings. However, adjusting the *z*-plane capture did not have any significant difference (Figure S2), and this allowed us to capture the bacteria on a fixed plane. One major issue with the use of fluorescent protein is photobleaching. It is the process by which repeated cycling of the fluorophore between ground and excited states eventually leads to molecular damage with a gradual reduction of fluorescence emission intensity from a sample over time.[39] By adjusting the transmission intensity of the lamp (Nikon, C-HGFI HG Fiber Illuminator "Intensilight" MBF72655), different droplets with fluorescent *E. coli* were constantly exposed to light for 30 min over a 1.5 h period under the two settings, i.e., ND32 (1/32 transmittance power) and ND1 (full transmittance power). The degradation of the fluorophore occurred quickly for ND1 (within 10 min) compared to ND32 degradation, which was much slower (Figure 4b). Although photobleaching occurred, by using a lower transmittance, degradation slowed down, which allowed for a longer measuring time to track the growth of *E. coli*. Fixing the camera setting and using a low power allowed us to obtain a higher *E. coli* growth with more accurate results.

Effect of Electric Fields. To determine how different voltages may affect growth, the encapsulated *E. coli* droplets that were trapped between the electrodes were exposed to final output sinusoidal voltages of 100, 200, and 400 V_{rms}. It was previously shown that an AC electric field can induce droplet deformation.[34] Therefore, we decided to use a sinusoidal voltage at a frequency of 50 kHz, as the droplet shape at low frequencies of 20 kHz and below was unstable and the droplet deformation was independent of frequency above 60 kHz. It was also shown that the deformation of droplets became stronger with increasing electric field intensity. In our case, droplets were exposed to increasing intensity of final output (100, 200, and 400 V_{rms}), which also showed an increase in deformation (the diameter of the droplet became smaller) (Figure 5a). However, voltages higher than 400 V_{rms} gave similar deformation (approximately 116 μm); thus, 400 V_{rms} was fixed as the upper limit. The droplets were exposed to an electric field for 30 min, and a 1 min recording of the fluorescent droplet was done. Previous studies have shown that electrostimulation of bacteria reduced the proliferation efficiency at a higher AC electric field (5 V/cm at 10 MHz).[40,41] However, electric currents were known to induce changes in DNA synthesis, protein synthesis, and membrane permeability.[42] To minimize bacterial cell damage due to electric currents, the electrodes were isolated from the fluidic channel (Figure 1), providing insulation against the electric current, and we used oil as the continuous phase as it is a poor conductor of electricity. It was observed that there was an increase in fluorescence intensity for all of the three settings over 3 h (Figure 5b). This showed that the exposure of cells to such an electric field did not affect their growth. Although there was no significant difference between the control and experimental growth rates, bacteria exposed to various voltages appeared to grow slightly faster. Besides comparing between the control and experimental groups, the relationship between voltage parameters and fluorescence was also analyzed by an R^2 plot (Figure S3). However, the overall slope gradient for each

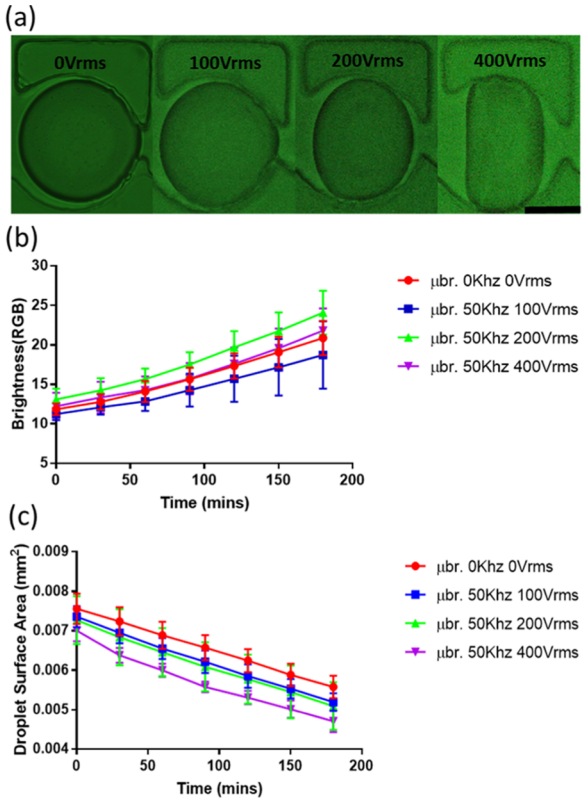

Figure 5. Effects of various electric fields (EF) applied on the droplets encapsulating *E. coli*. (A) Droplet deformation with various voltages. Scale bar = 100 μm. (B) EF effect of *E. coli* growth. T-test analysis with control shows no significant difference between increasing voltage with the control (n = 3). (C) Droplet size over a 3 h period at 25 °C for various voltages.

timepoint is similar and not significantly different. With increasing voltage, the droplets became narrower (Figure 5a), possibly allowing better mixing of bacterial cells and nutrients,[34] thus improving the bacterial growth. The electrokinetic effects from the electric field can also play a role in concentrating bacteria within the droplet.[43−45] Most droplets followed the same trend (gradually decreasing approximately 25% over time) except for droplets exposed to 50 kHz and 400 V_{rms}, which showed a greater drop in size (Figure 5c). A possibility could be that the turning off and on of the generator for recording the results at every 30 min interval might have caused the "stretching" of droplets and, in doing so, the droplets lose media in the process. Our initial results showed that a prolonged exposure to an AC electric field does not affect the growth rate of *E. coli*, but higher voltages may reduce the droplet size faster. Next, we determined how oscillation of the droplet might improve the growth rate by applying a square-wave modulation of 1 Hz.

Effect of Oscillation. It was shown that the rate of growth and final cell number of *E. coli* increased when the liquid culture media are shaken.[2,46] In bulk culture assays, liquid media must be aerated to provide dissolved oxygen and proper mixing of media. The commonly used way is vigorous stirring or shaking of the culture flask. One important factor to consider is the surface area of the liquid. By vigorously agitating the liquid media, these mixing techniques provide better mixing and minimize areas of high or low nutrient concentration. To provide a shaking effect for our μBR, droplet

https://dx.doi.org/10.1021/acsbiomaterials.0c00292
ACS Biomater. Sci. Eng. 2020, 6, 3630−3637

manipulation was done by applying a square-wave modulation of different frequencies, which enabled us to create an oscillation effect possibly mixing cells and nutrients. The use of an electric field allowed for precise control on multiple droplets, causing them to deform and return to their original shape quickly. Using droplets, we hypothesized that with higher droplet deformation rates and faster speeds, better agitation may occur, leading to a faster growth rate. For simulating faster speeds, the oscillation rate was increased by changing the frequency of the square-wave modulation magnitude from 10 to 100 Hz to oscillate the droplet faster (Supplementary Video S1). Results indicated that there was no change in the growth rate with increasing frequency (Figure 6).

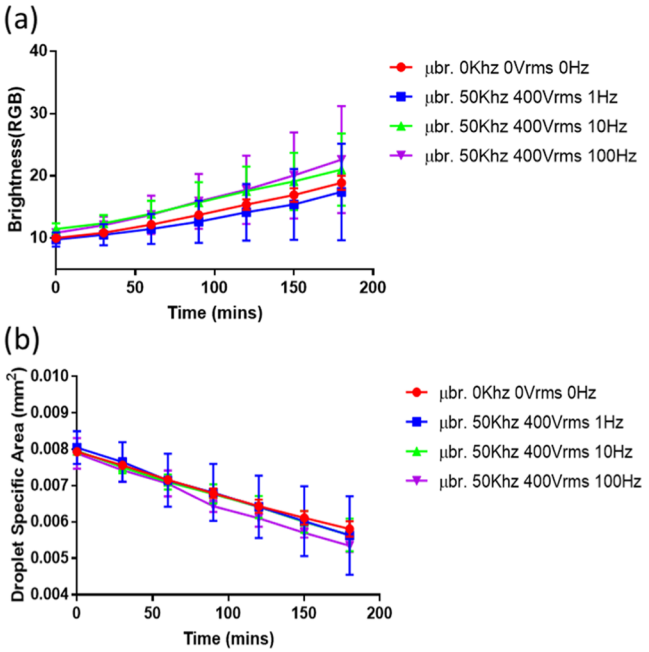

Figure 6. Effects of oscillation on *E. coli* growth. (a) Increase in oscillation over a 3 h period. (b) Decrease in droplet size over 3 h at 25 °C for various frequencies.

It is possible that at 1 and 10 Hz, the speed might not be fast enough, while at 100 Hz, the response time of the droplet deformation might be too fast for any deformation to take place. Another possible reason is that the droplet may not contain enough nutrients for the cell to grow quickly. The droplet size decreases gradually with increasing modulation, unlike the deformation in the previous experiment (Figure 5c). To summarize, our microfluidics microbioreactor provides an environment that allows upscaling and quick visualization of *E. coli* cell growth. Initial results showed that electric field did not affect growth while providing an additional option for manipulating droplets.

Comparison of *E. coli* Growth in *μ*br and in Shake Flasks. Our initial results showed that increasing oscillation did not significantly affect the encapsulated bacteria growth compared to the control. The next step was to determine the duration in which the microorganism can grow in the droplet and whether other growth stages appear during that time. The reason is that the cells that grow healthy initially will slow down when they come into contact with a new environment; therefore, a lag phase is produced.[47] For a comparative study, *E. coli* was first grown in a shake flask at 25 and 37 °C, with 37 °C being the optimal temperature for *E. coli* growth. The cells were measured at 1 h intervals to get their optical density. Figure 7a shows that the cells grown at 37 °C were able to

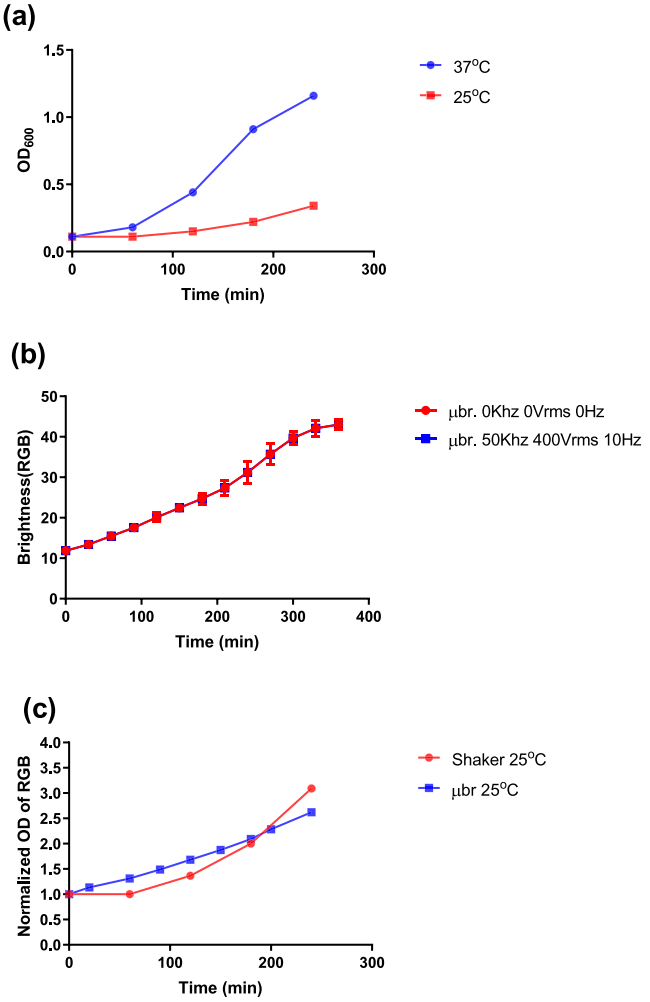

Figure 7. Comparisons of the growth of *E. coli* in shake flasks and in droplet microfluidic device *μ*br. (a) *E. coli* growth in shake flasks at 37 and 25 °C; (b) *E. coli* growth in *μ*br with and without oscillation at 25 °C; and (c) *E. coli* growth in shake flasks vs *μ*br at 25 °C.

reach a stationary phase after 4 h while those grown at room temperature slowly entered the log phase. From the oscillation experiments (Figure 6), we noted that there was a slight increase in growth for 50 kHz 400 V_{rms} 10 Hz and decided to run with this setting for a longer period. To prevent the droplets from shrinking too quickly, they were incubated at room temperature. The droplet size was found to decrease (approximately 60%) after a 6 h period (Figure S4). From this result (Figure 7b), it seemed that oscillating droplets for a longer period (6 h) did not have any significant effect on bacteria growth. Interestingly, we were able to obtain a standard growth curve similar to that of a shake flask with cells grown at 37 °C rather than at room temperature. As mentioned previously, one major advantage of using droplets as a microbioreactor is its stochastic confinement.[6] This confinement allows microorganisms or their metabolites[48,49] to accumulate faster, resulting, in our case, in a faster growth of *E. coli* (Figure 7c). However, it is important to note that further experimentation needs to be done to confirm that the cell

https://dx.doi.org/10.1021/acsbiomaterials.0c00292
ACS Biomater. Sci. Eng. 2020, 6, 3630−3637

behavior is similar to that in the shake flask at the gene expression level due to the different temperatures used.

CONCLUSIONS

Droplet microfluidics provides numerous advantages for studying single or a small amount of microorganisms in their own tiny liquid compartment. In this paper, we demonstrated for the first time an AC electric-field-induced droplet oscillation μBr for microorganism cultivation. We have shown the possibility of a microfluidic platform generating, sorting, and trapping cell-encapsulated droplets. By varying the electric field voltage and frequency, we were able to manipulate droplets, creating an oscillation (shaking effect) of *E. coli*. It was also observed that the AC electric field did not affect *E. coli* growth, enabling further work with our design. A comparison between a shake flask and our droplet microfluidic device showed that encapsulated droplets grown at room temperature were able to obtain a standard growth curve similar to that obtained using a shake flask at 37 °C within 6 h, a much faster rate than the growth in the shake flask at room temperature. This microfluidic device can provide researchers with another solution that is high throughput and cost-effective as well as provide a variable environment for cell analysis. However, more experiments must be carried out with different cell types to determine their individual optimal conditions for ideal results. We foresee that this device has the potential for making droplet microfluidics a better alternative for research as it provides a dynamic environment for biological studies.

ASSOCIATED CONTENT

Supporting Information

The Supporting Information is available free of charge at https://pubs.acs.org/doi/10.1021/acsbiomaterials.0c00292.

Droplet sorting graph, image processing procedures, other camera settings, and R2 plot between voltage and fluorescence for electric fields (PDF)

Video of droplet oscillations at different frequencies of 0.5, 1, and 100 Hz, and droplet size after 6 h (AVI)

AUTHOR INFORMATION

Corresponding Authors

Say Hwa Tan − *Queensland Micro- and Nanotechnology Centre, Griffith University, Brisbane, QLD 4111, Australia;* orcid.org/0000-0002-9764-7868; Email: sayhwa.tan@griffith.edu.au

Chun-Xia Zhao − *Australian Institute for Bioengineering and Nanotechnology, The University of Queensland, St. Lucia, QLD 4072, Australia;* orcid.org/0000-0002-3365-3759; Email: z.chunxia@uq.edu.au

Authors

Chee Meng Benjamin Ho − *Queensland Micro- and Nanotechnology Centre, Griffith University, Brisbane, QLD 4111, Australia*

Qi Sun − *Australian Institute for Bioengineering and Nanotechnology, The University of Queensland, St. Lucia, QLD 4072, Australia*

Adrian J. T. Teo − *Queensland Micro- and Nanotechnology Centre, Griffith University, Brisbane, QLD 4111, Australia*

David Wibowo − *Centre for Cell Factories and Biopolymers, Griffith Institute for Drug Discovery, Griffith University, Nathan, QLD 4111, Australia;* orcid.org/0000-0001-6919-3355

Yongsheng Gao − *School of Engineering, Griffith University, Brisbane, QLD 4111, Australia*

Jun Zhou − *School of Information and Communication Technology, Griffith University, Brisbane, QLD 4111, Australia*

Yanyi Huang − *Department of Advanced Materials and Nanotechnology, College of Engineering, Peking University, 100084 Beijing, China;* orcid.org/0000-0002-7297-1266

Complete contact information is available at: https://pubs.acs.org/10.1021/acsbiomaterials.0c00292

Author Contributions

[▽]C.M.B.H. and Q.S. have contributed equally to this work.

Notes

The authors declare no competing financial interest.

ACKNOWLEDGMENTS

C.X.Z. acknowledges financial support from the Australian Research Council through the award of an ARC Future Fellowship (FT140100726). S.H.T. acknowledges the support of the Australian Research Council (ARC) Discovery Early Career Researcher Award (DECRA) (DE170100600). This work was performed in part at the Queensland node of the Australian National Fabrication Facility funded under the Australian Government's NCRIS program.

REFERENCES

(1) Hegab, H. M.; Elmekawy, A.; Stakenborg, T. Review of microfluidic microbioreactor technology for high-throughput submerged microbiological cultivation. *Biomicrofluidics* **2013**, *7*, No. 021502.

(2) Bates, M. K.; Phillips, D. S.; O'Bryan, J. Shaker agitation rate and orbit affect growth of cultured bacteria. *Thermo Fisher Scientific ANSHORBGRT* **2016**, 816.

(3) Betts, J.; Warr, S.; Finka, G.; Uden, M.; Town, M.; Janda, J.; Baganz, F.; Lye, G. Impact of aeration strategies on fed-batch cell culture kinetics in a single-use 24-well miniature bioreactor. *Biochem. Eng. J.* **2014**, *82*, 105−116.

(4) Chen, X.; Liang, Z.; Li, D.; Xiong, Y.; Xiong, P.; Guan, Y.; Hou, S.; Hu, Y.; Chen, S.; Liu, G.; et al. Microfluidic dielectrophoresis device for trapping, counting and detecting *Shewanella oneidensis* at the cell level. *Biosens. Bioelectron.* **2018**, *99*, 416−423.

(5) Weuster-Botz, D.; Stevens, S.; Hawrylenko, A. Parallel-operated stirred-columns for microbial process development. *Biochem. Eng. J.* **2002**, *11*, 69−72.

(6) Kaminski, T. S.; Scheler, O.; Garstecki, P. Droplet microfluidics for microbiology: techniques, applications and challenges. *Lab Chip* **2016**, *16*, 2168−2187.

(7) Zhao, C. X.; Dwyer, M. D.; Yu, A. L.; Wu, Y.; Fang, S.; Middelberg, A. P. A simple and low-cost platform technology for producing pexiganan antimicrobial peptide in *E. coli*. *Biotechnol. Bioeng.* **2015**, *112*, 957−64.

(8) Wibowo, D.; Yang, G. Z.; Middelberg, A. P.; Zhao, C. X. Non-chromatographic bioprocess engineering of a recombinant mineralizing protein for the synthesis of silica nanocapsules. *Biotechnol. Bioeng.* **2017**, *114*, 335−343.

(9) Duetz, W. A.; Rüedi, L.; Hermann, R.; O'Connor, K.; Büchs, J.; Witholt, B. Methods for intense aeration, growth, storage, and replication of bacterial strains in microtiter plates. *Appl. Environ. Microbiol.* **2000**, *66*, 2641−2646.

(10) Warringer, J.; Blomberg, A. Automated screening in environmental arrays allows analysis of quantitative phenotypic profiles in *Saccharomyces cerevisiae*. *Yeast* **2003**, *20*, 53−67.

(11) Klein, A. M.; Mazutis, L.; Akartuna, I.; Tallapragada, N.; Veres, A.; Li, V.; Peshkin, L.; Weitz, D. A.; Kirschner, M. W. Droplet barcoding for single-cell transcriptomics applied to embryonic stem cells. *Cell* **2015**, *161*, 1187−1201.
(12) Whitesides, G. M. The origins and the future of microfluidics. *Nature* **2006**, *442*, 368.
(13) Weibel, D. B.; DiLuzio, W. R.; Whitesides, G. M. Microfabrication meets microbiology. *Nat. Rev. Microbiol.* **2007**, *5*, 209.
(14) Saleh-Lakha, S.; Trevors, J. T. Perspective: microfluidic applications in microbiology. *J. Microbiol. Methods* **2010**, *82*, 108−111.
(15) Lee, J.-H.; Kaplan, J. B.; Lee, W. Y. Microfluidic devices for studying growth and detachment of *Staphylococcus epidermidis* biofilms. *Biomed. Microdevices* **2008**, *10*, 489−498.
(16) Ran, R.; Sun, Q.; Baby, T.; Wibowo, D.; Middelberg, A. P. J.; Zhao, C. X. Multiphase microfluidic synthesis of micro- and nanostructures for pharmaceutical applications. *Chem. Eng. Sci.* **2017**, *169*, 78−96.
(17) Wang, H. F.; Ran, R.; Liu, Y.; Hui, Y.; Zeng, B. J.; Chen, D.; Weitz, D. A.; Zhao, C. X. Tumor-Vasculature-on-a-Chip for Investigating Nanoparticle Extravasation and Tumor Accumulation. *ACS Nano* **2018**, *12*, 11600−11609.
(18) Zanzotto, A.; Szita, N.; Boccazzi, P.; Lessard, P.; Sinskey, A. J.; Jensen, K. F. Membrane-aerated microbioreactor for high-throughput bioprocessing. *Biotechnol. Bioeng.* **2004**, *87*, 243−254.
(19) Boccazzi, P.; Zhang, Z.; Kurosawa, K.; Szita, N.; Bhattacharya, S.; Jensen, K. F.; Sinskey, A. J. Differential gene expression profiles and real-time measurements of growth parameters in *Saccharomyces cerevisiae* grown in microliter-scale bioreactors equipped with internal stirring. *Biotechnol. Prog.* **2006**, *22*, 710−717.
(20) Zanzotto, A.; Boccazzi, P.; Gorret, N.; Van Dyk, T. K.; Sinskey, A. J.; Jensen, K. F. In situ measurement of bioluminescence and fluorescence in an integrated microbioreactor. *Biotechnol. Bioeng.* **2006**, *93*, 40−47.
(21) Steinhaus, B.; Garcia, M. L.; Shen, A. Q.; Angenent, L. T. A portable anaerobic microbioreactor reveals optimum growth conditions for the methanogen *Methanosaeta concilii*. *Appl. Environ. Microbiol.* **2007**, *73*, 1653−1658.
(22) Edlich, A.; Magdanz, V.; Rasch, D.; Demming, S.; Aliasghar Zadeh, S.; Segura, R.; Kähler, C.; Radespiel, R.; Büttgenbach, S.; Franco-Lara, E. Microfluidic reactor for continuous cultivation of Saccharomyces cerevisiae. *Biotechnol. Prog.* **2010**, *26*, 1259−1270.
(23) Alam, M. N. H. Z.; Schäpper, D.; Gernaey, K. V. Embedded resistance wire as a heating element for temperature control in microbioreactors. *J. Micromech. Microeng.* **2010**, *20*, No. 055014.
(24) van Leeuwen, M.; Krommenhoek, E. E.; Heijnen, J. J.; Gardeniers, H.; van der Wielen, L. A.; Van Gulik, W. M. Aerobic batch cultivation in micro bioreactor with integrated electrochemical sensor array. *Biotechnol. Prog.* **2010**, *26*, 293−300.
(25) Luo, X.; Shen, K.; Luo, C.; Ji, H.; Ouyang, Q.; Chen, Y. An automatic microturbidostat for bacterial culture at constant density. *Biomed. Microdevices* **2010**, *12*, 499−503.
(26) Mahler, L.; Tovar, M.; Weber, T.; Brandes, S.; Rudolph, M. M.; Ehgartner, J.; Mayr, T.; Figge, M. T.; Roth, M.; Zang, E. Enhanced and homogeneous oxygen availability during incubation of microfluidic droplets. *RSC Adv.* **2015**, *5*, 101871−101878.
(27) Sun, Q.; Tan, S. H.; Chen, Q. S.; Ran, R.; Hui, Y.; Chen, D.; Zhao, C. X. Microfluidic Formation of Coculture Tumor Spheroids with Stromal Cells As a Novel 3D Tumor Model for Drug Testing. *ACS Biomater. Sci. Eng.* **2018**, *4*, 4425−4433.
(28) Leung, K.; Zahn, H.; Leaver, T.; Konwar, K. M.; Hanson, N. W.; Pagé, A. P.; Lo, C.-C.; Chain, P. S.; Hallam, S. J.; Hansen, C. L. A programmable droplet-based microfluidic device applied to multiparameter analysis of single microbes and microbial communities. *Proc. Natl. Acad. Sci. USA* **2012**, *109*, 7665−7670.
(29) Sesen, M.; Alan, T.; Neild, A. Droplet control technologies for microfluidic high throughput screening (μHTS). *Lab Chip* **2017**, *17*, 2372−2394.
(30) Headen, D. M.; García, J. R.; García, A. J. Parallel droplet microfluidics for high throughput cell encapsulation and synthetic microgel generation. *Microsyst. Nanoeng.* **2018**, *4*, 1−9.
(31) Hol, F. J.; Dekker, C. Zooming in to see the bigger picture: Microfluidic and nanofabrication tools to study bacteria. *Science* **2014**, *346*, No. 1251821.
(32) Liu, Z.; Banaei, N.; Ren, K. Microfluidics for Combating Antimicrobial Resistance. *Trends Biotechnol.* **2017**, *35*, 1129−1139.
(33) Tan, S. H.; Nguyen, N.-T.; Chua, Y. C.; Kang, T. G. Oxygen plasma treatment for reducing hydrophobicity of a sealed polydimethylsiloxane microchannel. *Biomicrofluidics* **2010**, *4*, No. 032204.
(34) Xi, H.-D.; Guo, W.; Leniart, M.; Chong, Z. Z.; Tan, S. H. AC electric field induced droplet deformation in a microfluidic T-junction. *Lab Chip* **2016**, *16*, 2982−2986.
(35) Huebner, A.; Bratton, D.; Whyte, G.; Yang, M.; Demello, A. J.; Abell, C.; Hollfelder, F. Static microdroplet arrays: a microfluidic device for droplet trapping, incubation and release for enzymatic and cell-based assays. *Lab Chip* **2009**, *9*, 692−698.
(36) Courtois, F.; Olguin, L. F.; Whyte, G.; Theberge, A. B.; Huck, W. T.; Hollfelder, F.; Abell, C. Controlling the retention of small molecules in emulsion microdroplets for use in cell-based assays. *Anal. Chem.* **2009**, *81*, 3008−3016.
(37) Dewan, A.; Kim, J.; McLean, R. H.; Vanapalli, S. A.; Karim, M. N. Growth kinetics of microalgae in microfluidic static droplet arrays. *Biotechnol. Bioeng.* **2012**, *109*, 2987−2996.
(38) Cormack, B. P.; Valdivia, R. H.; Falkow, S. FACS-optimized mutants of the green fluorescent protein (GFP). *Gene* **1996**, *173*, 33−38.
(39) Bridle, H. Chapter Five - Optical Detection Technologies for Waterborne Pathogens. *Waterborne Pathogens*; Bridle, H., Ed.; Academic Press: Amsterdam, 2014; pp 119−145.
(40) Giladi, M.; Porat, Y.; Blatt, A.; Wasserman, Y.; Kirson, E. D.; Dekel, E.; Palti, Y. Microbial growth inhibition by alternating electric fields. *Antimicrob. Agents Chemother.* **2008**, *52*, 3517−3522.
(41) Giladi, M.; Porat, Y.; Blatt, A.; Shmueli, E.; Wasserman, Y.; Kirson, E. D.; Palti, Y. Microbial growth inhibition by alternating electric fields in mice with *Pseudomonas aeruginosa* lung infection. *Antimicrob. Agents Chemother.* **2010**, *54*, 3212−3218.
(42) Nakanishi, K.; Tokuda, H.; Soga, T.; Yoshinaga, T.; Takeda, M. Effect of electric current on growth and alcohol production by yeast cells. *J. Ferment. Bioeng.* **1998**, *85*, 250−253.
(43) Liao, D. S.; Raveendran, J.; Golchi, S.; Docoslis, A. Fast and sensitive detection of bacteria from a water droplet by means of electric field effects and micro-Raman spectroscopy. *Sens. Bio-Sens. Res.* **2015**, *6*, 59−66.
(44) Chen, X.; Liang, Z.; Li, D.; Xiong, Y.; Xiong, P.; Guan, Y.; Hou, S.; Hu, Y.; Chen, S.; Liu, G.; Tian, Y. Microfluidic dielectrophoresis device for trapping, counting and detecting Shewanella oneidensis at the cell level. *Biosens. Bioelectron.* **2018**, *99*, 416−423.
(45) Lagally, E. T.; Lee, S.-H.; Soh, H. Integrated microsystem for dielectrophoretic cell concentration and genetic detection. *Lab Chip* **2005**, *5*, 1053−1058.
(46) Juergensmeyer, M. A.; Nelson, E. S.; Juergensmeyer, E. A. Shaking alone, without concurrent aeration, affects the growth characteristics of *Escherichia coli*. *Lett. Appl. Microbiol.* **2007**, *45*, 179−183.
(47) Sezonov, G.; Joseleau-Petit, D.; D'Ari, R. *Escherichia coli* Physiology in Luria-Bertani Broth. *J. Bacteriol.* **2007**, *189*, 8746−8749.
(48) Boedicker, J. Q.; Vincent, M. E.; Ismagilov, R. F. Microfluidic Confinement of Single Cells of Bacteria in Small Volumes Initiates High-Density Behavior of Quorum Sensing and Growth and Reveals Its Variability. *Angew. Chem., Int. Ed.* **2009**, *48*, 5908−5911.
(49) Boedicker, J. Q.; Li, L.; Kline, T. R.; Ismagilov, R. F. Detecting bacteria and determining their susceptibility to antibiotics by stochastic confinement in nanoliter droplets using plug-based microfluidics. *Lab Chip* **2008**, *8*, 1265−1272.

https://dx.doi.org/10.1021/acsbiomaterials.0c00292
ACS Biomater. Sci. Eng. 2020, 6, 3630−3637